WFDC1/ps20: A host factor that influences the neutrophil response to murine hepatitis virus (MHV) 1 infection

Erin Rogers [a,b,1], Ben X. Wang [a,b,1], Zhu Cui [b], David R. Rowley [c], Steven J. Ressler [c], Annapurna Vyakarnam [d], Eleanor N. Fish [a,b,*]

[a] Toronto General Research Institute, Division of Cell and Molecular Biology, University Health Network, 67 College Street, Toronto, Ontario, Canada M5G 2M1
[b] Department of Immunology, University of Toronto, 1 King's College Circle, Toronto, Ontario, Canada, M5S 1A8
[c] Department of Molecular & Cellular Biology, Baylor College of Medicine, One Baylor Plaza, Houston, TX 77030, USA
[d] Department of Infectious Diseases, King's College London, Borough Wing, Guy's Hospital, London SE1 9RT, UK

ABSTRACT

The whey acidic protein family member, WFDC1/ps20 is a permissivity factor in HIV infection. Herein we describe a contrasting role for ps20 in limiting MHV-1 infection. Intranasal MHV-1 infection produces a respiratory infection in mice. Using ps20 knockout mice we provide evidence that intranasal MHV-1 infection results in increased lung viral titers in ps20$^{-/-}$ compared to ps20$^{+/+}$ mice. Accompanying MHV-1 infection we observe an increase in the number of neutrophils infiltrating the BAL and an increase in the percentage of neutrophils in the lung draining lymph nodes of ps20$^{-/-}$ compared with ps20$^{+/+}$ mice. Gene expression levels for the neutrophil chemoattractants *CXCL1* and *CXCL2* are elevated in the lungs of ps20$^{-/-}$ mice post-MHV-1 infection. Characterization of the immune cell profile in naïve ps20$^{-/-}$ mice revealed an increase in circulating neutrophils compared to ps20$^{+/+}$ mice. No notable differences in other immune cell profiles were observed between the ps20$^{+/+}$ and ps20$^{-/-}$ mice. Accordingly, we examined MHV-1 infection of neutrophils and provide evidence that neutrophils isolated from ps20$^{-/-}$ mice are more susceptible to MHV-1 infection than neutrophils isolated from ps20$^{+/+}$ mice. These data suggest roles for ps20 in regulating expression of neutrophil-specific chemotactic factors, thereby potentially modulating neutrophil migration, and in modulating neutrophil susceptibility to MHV-1 infection.

© 2012 Elsevier B.V. All rights reserved.

1. Introduction

Whey acidic protein (WAP) domain-containing proteins are small proteins possessing proteinase inhibitor activity, antimicrobial activity, ATPase inhibitor activity and regulatory activity in cell proliferation (Bingle and Vyakarnam, 2008). Secretory leukocyte protease inhibitor (SLPI), elafin and WFDC1/ps20 are three members of this WAP family, characterized by the presence of a four-disulfide core (FDC) structure (Bingle and Vyakarnam, 2008; Bouchard et al., 2006; Hennighausen and Sippel, 1982a, b; Piletz et al., 1981; Simpson et al., 2000; Simpson and Nicholas, 2002). SLPI and elafin exhibit antiviral activity that is not associated with their anti-protease function (Bingle and Vyakarnam, 2008; Ma et al., 2004; McNeely et al., 1995): SLPI inhibits human immunodeficiency virus (HIV) infection of primary monocytes by binding to annexin II (Bingle et al., 2001; Doumas et al., 2005; Ma et al., 2004) and elafin exerts its antiviral activity by direct binding to HIV (Ghosh et al., 2009). Unlike elafin and SLPI, ps20 is a permissivity factor for HIV infection (Alvarez et al., 2007).

ps20, encoded by the *WFDC1* gene on human chromosome 16, is ubiquitously expressed at sites of potential pathogen infection, including memory CD4+ T cells, likely contributing to HIV adaptation to exploit ps20 as a permissivity factor by upregulating a key cell-surface adhesion molecule, CD54 (Alvarez et al., 2007; Larsen et al., 2000). The interaction of CD54 with LFA-1 is known to stabilize HIV-1 fusion to targets cells, thereby promoting HIV entry. Thus, in contrast to SLPI and elafin, ps20 functions to enhance viral infectivity, at least for HIV.

Mouse hepatitis virus type 1 (MHV-1) is a member of the *Coronaviridae* family of positive single-stranded RNA viruses. MHV-1 infects a wide variety of species, including humans, rodents, felines and birds (Gu and Korteweg, 2007; Spaan et al., 1988). MHV-1 is a mouse-specific coronavirus (Spaan et al., 1988). MHV strains enter host cells via endocytosis mediated by a virion spike protein binding to host carcinoembryonic antigen-related cell adhesion molecule 1(CEACAM-1a) (Compton et al., 1992; Perlman and Netland,

2009). In an earlier report we described a mouse model of respiratory MHV-1 infection, wherein A/J mice are more susceptible to intranasal respiratory MHV-1 infection than C57Bl/6 mice, associated with differences in the host innate immune response, specifically the interferon (IFN) response (Albuquerque et al., 2006; Baig and Fish, 2008). Subsequent publications have confirmed that variable sensitivity to MHV-1 infection is a consequence of the innate and adaptive immune responses (Khanolkar et al., 2009a) and that MHV infection inhibits IFN production (Zhou and Perlman, 2007). Notably, MHV-1-specific T and B cell responses exert protective effects that minimize morbidity in C57Bl/6 mice (Khanolkar et al., 2009a). Given the contribution of innate and adaptive immune responses to morbidity in MHV-1 infection of C57Bl/6 mice and the accumulating data that WAP proteins influence susceptibility to infection, employing ps20$^{+/+}$ and ps20$^{-/-}$ C57Bl/6 mice we examined the effects of ps20 on the immune response to MHV-1 infection. Our data reveal a hitherto unreported contribution of neutrophils to MHV-1 infection and describe how ps20 expression affects both neutrophil migration to MHV-1 infected lungs and draining lymph nodes (dLNs) and neutrophil susceptibility to infection, associated with effects on lung virus replication.

2. Materials and methods

2.1. Cells and antibodies

L2 fibroblasts were a gift from Dr. Gary Levy (University Health Network, Toronto, ON) and were maintained in Dulbecco's modified Eagle's medium (DMEM) supplemented with 10% fetal calf serum (FCS), 1000 U/mL penicillin, and 100 μg/mL streptomycin. Skin fibroblast cells were generated from C57Bl/6 ps20$^{+/+}$ and ps20$^{-/-}$ mice. Mice were euthanized and sections of hairless skin removed, minced and seeded in 60 mm plates with 20% FCS DMEM for 7 days. Adherent fibroblasts were passaged.

The generation and characterization of the IG7 IgG1 monoclonal antibody (mAb) was as previously described (Alvarez et al., 2007). Specificity was confirmed using an enzyme-linked immunosorbent assay (ELISA) to recognize the immunizing peptide, full-length ps20. IG7 anti-ps20 fragmented antibodies (FAbs) and control IgG1 FAbs were produced by BioservUK Ltd. (Sheffield, UK). Control FAb was generated from XCIII-1F8-D7 08041723-anti-Leishmania (L) pifanoi Amastigote IgG1 hybridomas (Sigma). Each hybridoma was scaled up in roller bottle flasks to 1 L and affinity purified on standard Protein G Sepharose. Each Ab was concentrated to between 19–26 mg/ml and digested with immobilized papain (Pierce; 20341; KG135117) at 37 °C for 7 h with mixing. Samples were then diluted in 10 mM Tris HCl, pH7.5 and separated from immobilized papain by centrifugation. The FAb fragment was then purified by Protein A binding, filter sterilized and stored at 4 °C. Purity was confirmed by 1-D gel electrophoresis.

2.2. Mice

C57Bl/6. ps20$^{+/-}$ mice were provided by Dr. D. Rowley (Baylor College of Medicine, Houston, TX). These mice were generated through replacement of exon 1 of the WFDC1 gene with a LacZ gene at the WFDC1 ATG start codon. The LacZ-PGK-neo cassette introduced an EcoRV site, which was used for screening by Southern analysis. To confirm deletion of WFDC1 and insertion of LacZ, genomic DNA was digested with EcoRV and probed with a Spe1-Apa 1.3 kb probe. The ps20$^{-/-}$ allele is 6.5 kb, and the ps20$^{+/+}$ allele is 9.5 kb. The screened ps20$^{-/-}$ gene constructs were inserted into a 129 mouse blastocyte by electroporation and subsequently implanted into a C57Bl/6 ps20$^{+/+}$ female host. Pups were subsequently backcrossed to a C57Bl/6 background using a speed congenic approach. Briefly, low-density single-nucleotide polymorphism (SNP) analysis (The Center for Applied Genomics, Toronto, ON) was performed on tail-snip DNA from the pups of each progeny litter. Mice exhibiting the highest SNP homology to C57Bl/6 were selected for subsequent breeding. Screening was completed until mice were >98% homologous to C57Bl/6 mice. A/J and C57Bl/6 mice, aged 6–8 weeks were purchased from The Jackson Laboratory (Bar Harbor, ME). Mice were bred and housed in a pathogen-free environment and all experiments were approved by the Animal Care Committee of the Toronto General Research Institute.

2.3. Cell fractionation

For immune cell analysis of peripheral blood (PB), ps20$^{-/-}$ and ps20$^{+/+}$ mice were anesthetized with 300 μL of isoflurane and a cardiac puncture was performed to collect 700 μL of blood. RBCs were removed using ACK lysis buffer and peripheral blood mononuclear cells (PBMCs) were isolated by Ficoll gradient centrifugation at 800 g for 20 min. The spleen and lymph nodes (LNs) were harvested, mechanically disrupted, followed by enzymatic digestion with 1 μg/mL collagenase in 5% FCS and 30 μg/mL DNase in PBS, for 30 min. Cell suspensions were filtered through a 70 μm mesh, then centrifuged at 2000 rpm for 5 min. Bone marrow (BM) cells were obtained by flushing the marrow from femurs into PBS. RBCs were removed using ACK lysis buffer.

2.4. Neutrophil isolation

ps20$^{+/+}$ and ps20$^{-/-}$ mice were euthanized by cervical dislocation and their femurs and tibia harvested. The BM was flushed with PBS. Cells were resuspended at 1×10^8 cells/mL in the RoboSep Buffer (Stemcell). Neutrophils were purified using the Mouse Neutrophil Enrichment Kit (Stemcell) following the manufacturer's instructions. Neutrophils (up to 90% purity) were freshly isolated and used immediately.

2.5. Virus infections and titration

MHV-1 (provided by Dr. Gary Levy, UHN, Toronto) was propagated in 17CL1 cells. Viral titers were determined in L2 cells by plaque assay as previously described (Albuquerque et al., 2006).

ps20$^{+/+}$ and ps20$^{-/-}$ C57Bl/6 skin fibroblasts were seeded in 24-well culture plates at 2×10^5 cells/well, in 2 mL of DMEM and incubated at 37 °C in 5% CO$_2$. 16 h later the medium was removed, the cells washed with PBS, and 200 μL of DMEM containing MHV-1 at a multiplicity of infection (MOI) of 0.1 or 0.01 was added for one hour at 37 °C. Cells were washed with PBS and subsequently incubated with 500 μL of 2% FCS DMEM for a further 16 h. Progeny virus in the medium was titrated in L2 cells.

ps20$^{+/+}$ and ps20$^{-/-}$ neutrophils were seeded in 24-well culture plates at 1×10^6 cells/well, in 500 μL of 2% FCS RPMI and infected with MHV-1 at an MOI of 0.1 or 0.01 for 24 h at 37 °C in 5% CO$_2$. Progeny virus in the medium was titrated in L2 cells.

Female A/J or C57Bl/6 ps20$^{+/+}$ and ps20$^{-/-}$ mice, aged 6–8 weeks were anesthetized by intraperitoneal (ip) injection with a mixture of ketamine and xylazine and infected by intranasal instillation with 40 μL PBS containing 5×10^3 PFU of MHV-1. Mice were monitored daily for symptoms of disease: ruffled fur, tremors and lack of activity. Post-infection, mice were sacrificed by cervical dislocation. Lung dLNs were harvested for analysis by flow cytometry, and lung tissues were snap frozen in liquid nitrogen for immunohistochemistry, viral titration or for RNA extraction. One milliliter PBS was flushed through the lung to remove the infiltrating immune cells in a bronchial alveolar lavage (Albuquerque et al., 2006).

2.6. IFN treatment and viral cytopathic effect assay

ps20$^{+/+}$ and ps20$^{-/-}$ skin fibroblasts were seeded in 24-well culture plates at 2×10^5 cells/well, in 2 mL of 10% FCS DMEM and incubated at 37 °C in 5% CO_2. Prior to MHV-1 infection, cells were treated with either 10^3 or 10^4 U/mL IFN-α4. Medium containing progeny virus was harvested after 16 h and added to L2 cells in individual wells of 96-well culture plates. 24 h later virus-induced cytopathic effects (CPE) were quantitated using a crystal violet colorimetric assay as previously described (Fish et al., 1988; Zorzitto et al., 2006). Data are expressed as percent survival relative to untreated L2 cells.

2.7. RNA extraction, cDNA synthesis

Cells were lysed using RLT + β-mercaptoethanol using a Qiagen RNeasy mini kit (Qiagen), according to the manufacturer's protocol, with DNA digestion. RNA concentration was determined by UV absorbance at 260 nm. cDNAs were synthesized using 0.5 µg RNA, oligo-dT primers and Superscript III reverse transcriptase, according to the manufacturer's protocol (Invitrogen).

RNA was extracted from frozen mouse tissue using 500 µL Trizol (Invitrogen). The extracted RNA pellet was then washed with 1 mL of 75% ethanol and RNA concentration determined. cDNAs were synthesized using 0.5 µg of RNA as described above.

2.8. qRT–PCR

qRT–PCR was performed using a LightCycler® (Roche) and LightCycler® FastStart DNA Master SYBR Green^{PLUS} I kits (Roche). Reactions were in 20 µL containing 4 µL of LightCycler SYBR Green PLUS buffer, at a final concentration of $1\times$, 5 µL 100 µg/mL cDNA, 9 µL PCR-grade water and 1 µL each of 20 µM forward and reverse primers. PCR reactions were carried out under the following conditions: pre-incubation at 95 °C for 10 min, followed by 45 amplification cycles of denaturation at 95 °C for 10 s, annealing for 5 s at the T_M specified below, extension at 72 °C for 10 s, melting curve analysis at 65 °C for 15 s and continuous acquisition mode of 95 °C with a temperature transition rate of 0.1 °C/s. PCR products were cloned into a pCR 2.1-TOPO vector (Invitrogen), as per the manufacturer's protocol, to quantitate absolute transcript values. The cloned constructs were purified using the GenElute Plasmid Miniprep Kit (Sigma). A standard curve was generated for each construct by PCR amplification at log-fold dilutions of each product in the Light-Cycler® at the specified annealing temperature. Forward and reverse primer sets:

IFN-α4 (T_M 60 °C) F-5′-GCCATCCTTGTGCTAAGAG-3′,
R-3′-TCAAGAGGAGGTTCCTGCATCAC-3′;
IFN-β (T_M 60 °C): F-5′-TGCGTTCCTGCTGTGCTTCT-3′,
R-5′-TTGGATGGCAAAGGCAGTGT3′;
ISG15 (T_M 60 °C) F-5′-GTGTCAGAACTGAAGAAG-3′,
R-5′-CGTTCCTCACCAGGATGC-3′;
CXCL1(T_M 62 °C) F-5′-AACCGAAGTCATAGCCACAC-3′,
R-5′-CAGACGGTGCCATCAGAG-3′;
CXCL2 (T_M 62 °C) F-5′-CAGAAGTCATAGCCACTCTCAAG-3′,
R-5′-CTCCTTTCCAGGTCAGTTAGC-3′;
HPRT (T_M 60 °C) F-5′-ATCAGTCAACGGGGGACATA-3′,
R-5′-TTGCAACCTTAACCATTTTGG-3′.

2.9. Flow cytometry

Fluorochrome-labeled mAbs used were: FITC anti-CD69 (H1.2F3, eBioscience), PE anti-CD8 (53-6.7, BD), PE-Cy5 (PK136, eBioscience), APC anti-CD4 (GK1.5, eBioscience), PE-Cy7 anti-CD45 (30-F11, BD), APC-Cy7 anti-B220 (RA3-6B2, BD), Alexa Fluor®

700 anti-CD3 (17A2, eBioscience), FITC anti-CD11b (M1/70, BD), PE anti-CD80 (B7.1, eBioscience), PE-Cy5 anti-F4/80 (BM8, BD) APC anti-MHC-II (M5/114.15.2, eBioscience), PE-Cy7 anti-CD11c (N418, eBioscience), FITC anti-Ly6G (1A8, BD), PE anti-CD66a/CEA-CAM-1 (CC1, eBioscience), APC-Cy7, and APC anti-GR1 (RB6-8C5, BD). Appropriate isotype controls for surface stains were included (eBioscience & BD). Flow cytometry was performed using an LSR II or FACSCalibur flow cytometer (BD) and data were analyzed using FlowJo software (Tree Star, Inc.).

2.10. Immunohistology

Lungs from MHV-1-infected ps20$^{+/+}$and ps20$^{-/-}$ mice were sectioned at 14 µm in a cryostat (Leica, CM1850) and fixed onto microscope slides using methanol:acetone (50:50). Tissues were stained using FITC anti-Ly6G (1A8, BD), 4′-6-Diamidino-2-phenyl-indole (DAPI), or an appropriate isotype control antibody (BD). Slides were scanned with TISSUEscope (Huron Technologies) and analyzed using ImageScope (Aperio).

2.11. Neutrophil elastase assay

Human neutrophil elastase activity was measured as described (Simpson et al., 2001).

2.12. Reactive oxygen species detection assay

Intracellular ROS were detected using the fluorescent dye H_2-DCFDA, dichlorodrhydrofluorescein diacetate (Invitrogen). BM derived neutrophils from ps20$^{+/+}$ and ps20$^{-/-}$ mice were suspended in 10 µM H2DCFDA at room temperature for 30 min, washed with PBS and seeded in individual wells of 24-well culture plates at 1×10^6 cells/well and infected with MHV-1 at an MOI of 0.01 in a time course study (0–60 mins). Cells were then washed once in PBS containing 2% FCS and analyzed by FACS using the FL1 detector channel.

3. Results

3.1. ps20$^{-/-}$ mice have high circulating levels of neutrophils

At the outset we undertook to characterize the abundance and relative proportions of immune cell populations in the peripheral blood (PB) of ps20$^{+/+}$ and ps20$^{-/-}$ mice. In contrast to ps20$^{+/+}$ mice, we observe a significant increase in the number of GR1$^+$ neutrophils circulating in the PB of ps20$^{-/-}$ mice (ps20$^{+/+}$ = 21%; ps20$^{-/-}$ = 32%) (Fig. 1A, B). Analysis of other PB leukocyte populations, including F4/80$^+$ macrophages, CD3$^+$CD4$^+$ and CD3$^+$CD8$^+$ T cells, B220$^+$ B cells and NK1.1 NK cells, revealed no statistically significant differences between ps20$^{+/+}$ and ps20$^{-/-}$ mice (Fig. 1B).

Next, we examined the spleen, LN and BM compartments in the ps20$^{-/-}$ and ps20$^{+/+}$ mice, aged 6–8 weeks. Spleen, LNs, and BM were processed as described in Section 2.3. The proportion of cells isolated from each of the compartments examined was indistinguishable between ps20$^{+/+}$ and ps20$^{-/-}$ mice (Supplementary Fig. 1). In contrast to what we observe in the PB, we did not detect any differences in the percentage of leukocyte/lymphocyte populations between ps20$^{+/+}$ and ps20$^{-/-}$ mice for spleen, LN or BM (Fig. 1C–E). Similarly, our analysis of the structural architecture and cellularity in the LN and the spleen did not reveal any differences in tissue morphology between the ps20$^{+/+}$ and ps20$^{-/-}$ mice (Supplementary Fig. 2).

3.2. ps20. protects from MHV-1 infection in vitro

Skin fibroblast cell lines were derived from ps20$^{+/+}$ and ps20$^{-/-}$ mice as described in Section 2.1. Skin fibroblasts from ps20$^{+/+}$ mice
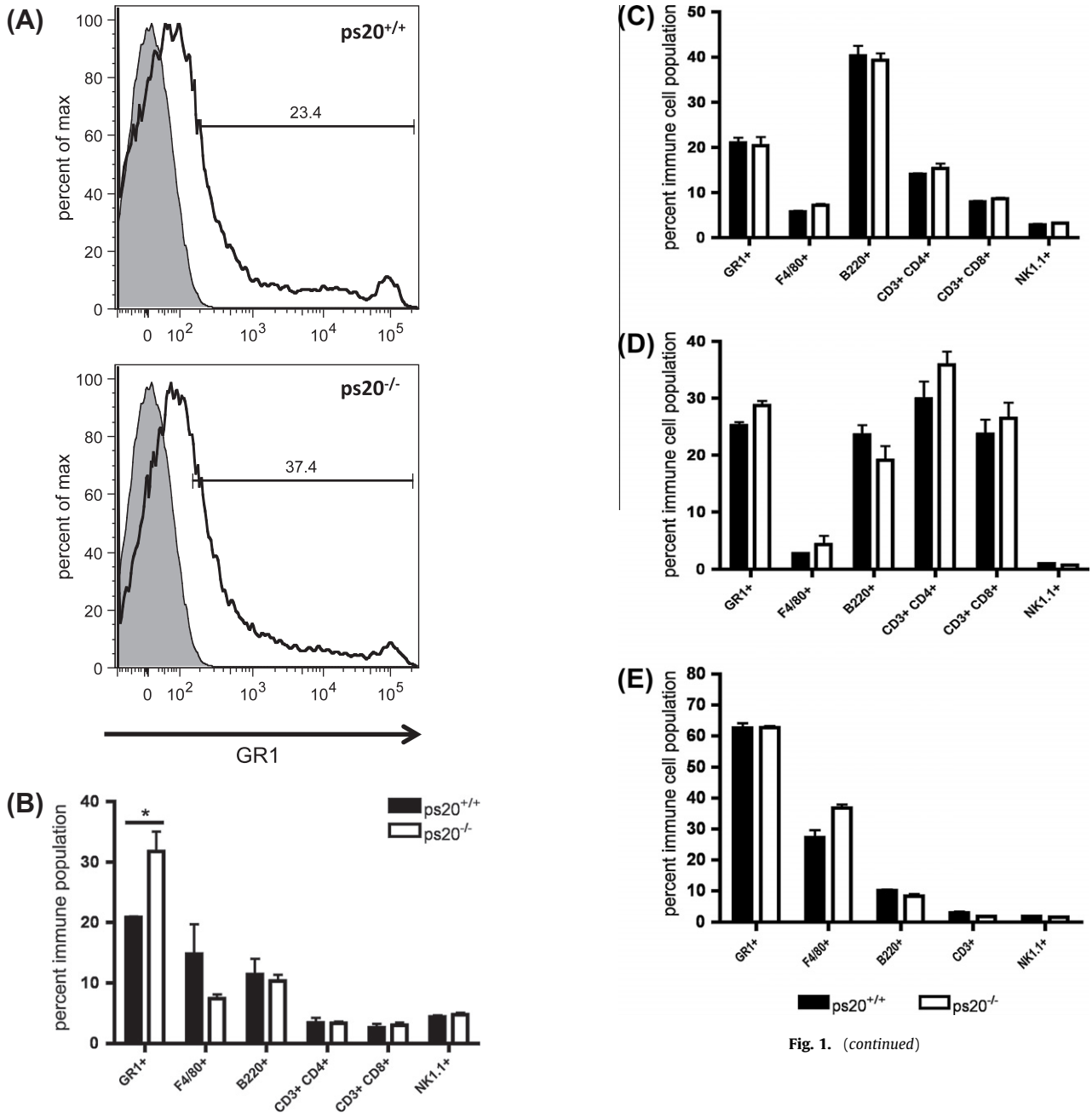
Fig. 1. Characterization of lineage specific markers for leukocyte populations in ps20$^{-/-}$ mice. Female C57Bl/6 ps20$^{+/+}$ and ps20$^{-/-}$ mice aged 6–8 weeks were euthanized and their LNs, spleen and BM were harvested and processed for FACS analysis. PB was harvested by cardiac puncture. Cells were isolated as described in Section 2.3 and stained with appropriate antibodies for specific immune cell markers. (A) Representative plots of cells stained for GR1 derived from the PB of ps20$^{+/+}$ and ps20$^{-/-}$ mice were generated based on isotype matched control antibodies. Lineage specific markers for different leukocyte populations were analyzed by FACS analysis, staining with antibodies specific for the indicated surface markers in the (B) PB, (C) spleen, (D) LN, (E) BM. Data are presented as the mean for each group ($n = 3$) ± standard error and are representative of one (BM) or two (PB, LNs, spleen) independent experiments and were analyzed using a Student's t test. $^{*}P < 0.05$.
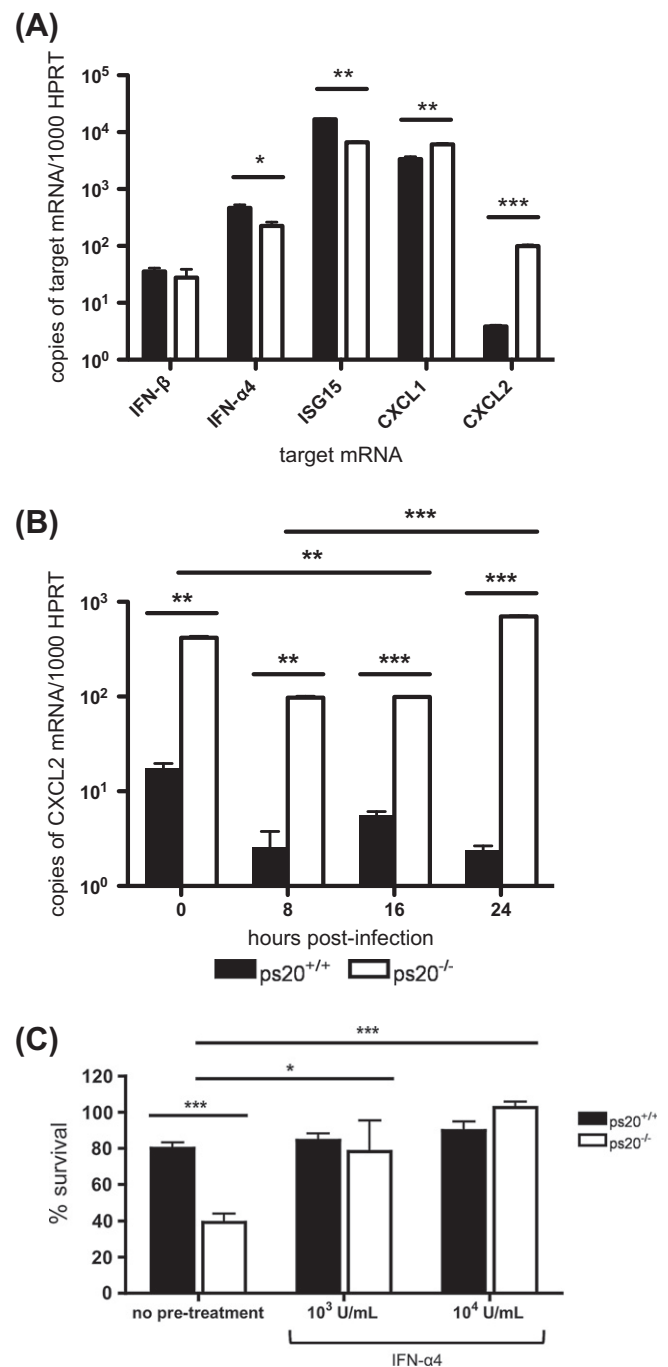
exhibit gene expression for ps20 (data not shown). In a first series of experiments we provide evidence that fibroblasts derived from ps20$^{-/-}$ mice are more sensitive to MHV-1 infection than fibroblasts from ps20$^{+/+}$ mice (Fig. 2A). Notably, MHV-1 infection of both ps20$^{+/+}$ and ps20$^{-/-}$ fibroblasts does not result in a cytopathic effect or induce apoptosis by 24 h post-infection, hence viral prog-

eny were measured in culture medium following infection of cells, using the L2 plaque assay as described (Section 2.5). To confirm that this outcome was a direct consequence of ps20 expression levels, we next examined the effects of treatment of ps20$^{+/+}$ fibroblasts with neutralizing antibodies to ps20, namely the anti-ps20 FAb IG7, on MHV-1 infection. Following a 1 h pre-treatment with IG7, ps20$^{+/+}$ fibroblasts were infected with MHV-1 at an MOI of 0.01 for 16 h. ps20$^{+/+}$ fibroblasts treated with IG7 exhibited higher viral titers compared with ps20$^{+/+}$ fibroblasts treated with either a control FAb or PBS (PBS mock-treated control ~12.75 PFU/mL; control IgG ~16.7 PFU/mL; IG7 ~535.4 PFU/mL) (Fig. 2B).

Given the data that an IFN response is critical in limiting MHV-1 infection, we next examined whether ps20 might affect gene expression for IFN-α4, IFN-β, and an IFN-inducible gene associated with an antiviral response, ISG15, thereby influencing sensitivity to infection. The induced gene expression levels of IFN-α4 and ISG15 are greater in the ps20$^{+/+}$ fibroblasts compared with the ps20$^{-/-}$ fibroblasts when infected with MHV-1 at an MOI of 0.1, although
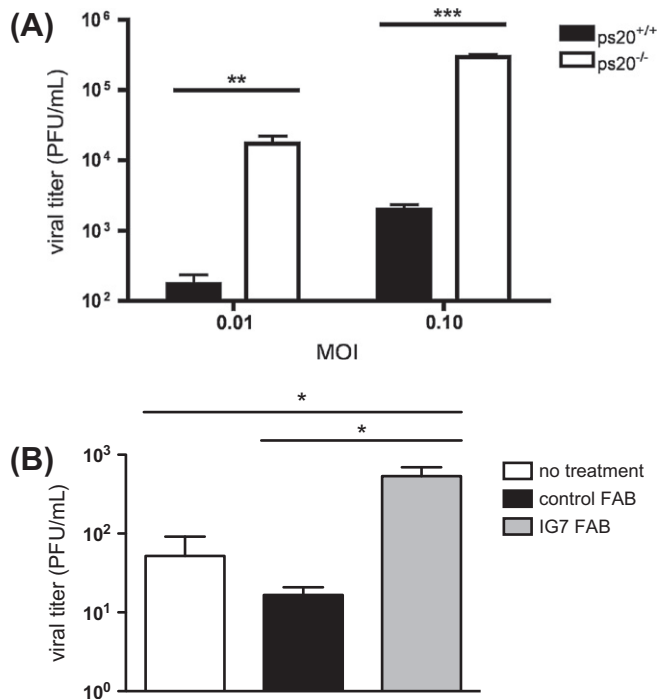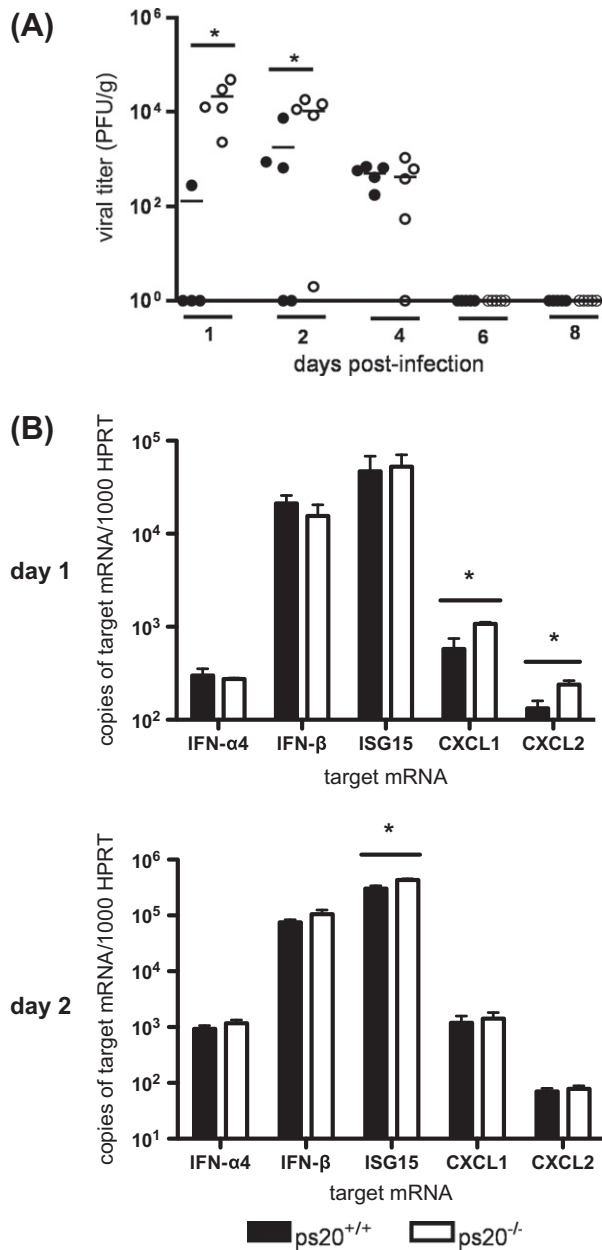
Fig. 2. ps20 expression limits MHV-1 infection in fibroblasts. Skin fibroblasts were derived from adult ps20$^{+/+}$ and ps20$^{-/-}$ mice and passaged *in vitro*. (A) Cultures were infected with MHV-1 at MOIs of 0.01 and 0.1 for 16 h, then viral titers determined as described in Section 2.5. (B) Fibroblasts derived from ps20$^{+/+}$ mice were either mock-treated (PBS), treated with an IgG control FAb antibody, or the ps20 neutralizing antibody, IG7, at 10 μg/mL for 1 h prior to challenge with MHV-1 (MOI of 0.01). 16 h later, viral titers were determined. Data are presented as the number of plaque forming units per mL (PFU/mL) for each group ($n = 3$) ± standard error and are representative of two independent experiments. Data were analyzed using a Student's *t* test. $^*P < 0.05$; $^{**}P < 0.01$; $^{***}P < 0.001$.

IFN-β gene expression is induced to comparable levels (Fig. 3A). Next we examined the gene expression levels for CXCL1 and CXCL2, chemokines with neutrophil chemoattractant activity. CXCL1 and CXCL2 gene expression levels are detectable post-infection in both the ps20$^{-/-}$ and ps20$^{+/+}$ fibroblasts, with greater CXCL1 and CXCL2 gene expression in the ps20$^{-/-}$ fibroblasts (Fig. 3A). In a more extensive time course study we observe that following MHV-1 infection CXCL2 gene expression is downregulated in ps20$^{+/+}$ fibroblasts (Fig. 3B). Notably, in the absence of ps20, basal levels of CXCL2 are higher in the ps20$^{-/-}$ fibroblasts and, following MHV-1 infection, although there is some downregulation in CXCL2 expression, by 24 h levels are elevated again and comparable to uninfected cells, in stark contrast to the ps20 sufficient fibroblasts (Fig. 3B). The implications are that ps20 may directly or indirectly regulate CXCL2 expression.

We next performed a set of *in vitro* experiments to examine whether treatment with IFN-α4 would provide protection against MHV-1 infection in ps20$^{-/-}$ fibroblasts. Specifically, as per our standard IFN antiviral assay, cells were treated with IFN for 16 h, then challenged with MHV-1. 16 h post-infection the culture medium was harvested and assayed for viral progeny using the CPE assay in L2 cells. Culture medium harvested from ps20$^{-/-}$ fibroblasts treated with IFN-α4 and then infected with MHV-1 at an MOI of 0.01 for 16 h is less cytopathic in L2 cells compared with medium from MHV-1 infected and untreated ps20$^{-/-}$ cells (Fig. 3C). These data suggest that the absence of ps20 does not affect an IFN response. As in Fig. 2A, we observe the protective effects of ps20 expression in the ps20$^{+/+}$ fibroblasts, in the absence of IFN treatment.

Fig. 3. ps20 expression effects on IFN and chemokine induction and an IFN-induced antiviral response. (A) ps20$^{-/-}$ and ps20$^{+/+}$ fibroblast cultures were infected with MHV-1 at an MOI of 0.1 for 16 h. Cellular RNA was extracted and cDNA was synthesized for qRT–PCR of the indicated genes. For each test group ($n = 3$) the copy number of the reference gene (HPRT) and the target gene (IFN-α4, IFN-β, ISG15, CXCL1 & CXCL2) were determined. (B) CXCL2 gene expression was further characterized in ps20$^{-/-}$ and ps20$^{+/+}$ fibroblast cultures infected with MHV-1 at an MOI of 0.1 for 8, 16, and 24 h. qRT–PCR data are presented as the copy number of the target gene relative to 1000 copies of HPRT, plotted as the mean copy number for each gene ± standard error. (A and B) are representative of three and two independent experiments respectively, and were analyzed using a Student's *t* test. (C) ps20$^{-/-}$ and ps20$^{+/+}$ fibroblast cultures were treated with IFN-α4 at the indicated doses 16 h prior to infection with MHV-1 at an MOI of 0.01. 16 h after infection with MHV-1, culture medium was harvested overlayed onto L2 cells, as described in Section 2.6. Data are presented as percent survival compared to control L2 cells treated with culture from uninfected fibroblasts (100% survival), plotted as the mean% survival ± standard error and are representative of two independent experiments and technical replicates ($n = 4$–8). Data were analyzed using a Student's *t* test. $^*P < 0.05$; $^{**}P < 0.01$; $^{***}P < 0.001$.

Fig. 4. ps20$^{-/-}$ mice exhibit increased susceptibility to respiratory MHV-1 infection. (A) Female ps20$^{+/+}$ and ps20$^{-/-}$ mice aged 6–8 weeks were infected by intranasal instillation with 5×10^3 PFU of MHV-1. Mice were sacrificed at the indicated time points and their lungs harvested for viral titration as described in Section 2.5. Data are presented as PFU/g of lung tissue for each mouse, with the mean of each group ($n = 5$) indicated by the solid black line and are representative of two independent experiments. Data were analyzed using a Student's t test. (B) Female and male ps20$^{+/+}$ and ps20$^{-/-}$ mice aged 6–8 weeks were infected by intranasal instillation with 5×10^3 PFU of MHV-1. Mice were sacrificed on days 1 and 2 post-infection and their lungs harvested, RNA extracted and cDNA synthesized. Gene expression levels for IFN-α4, IFN-β, ISG15, CXCL1, and CXCL2 were determined by qRT–PCR as described in Section 2.8. Data are presented as the copy number of the target gene relative to 1000 copies of HPRT, plotted as the mean copy number for each gene ± standard error. IFN-α4, IFN-β, and ISG15 data are representative of three independent experiments ($n = 3$–5) and CXCL1, and CXCL2 data are representative of a single experiment ($n = 3$). Data were analyzed using a Student's t test. *$P < 0.05$.

3.3. ps20 confers protection from MHV-1 infection in vivo

In subsequent *in vivo* studies, we compared the susceptibility of C57Bl/6 ps20$^{+/+}$ and ps20$^{-/-}$ mice to challenge with MHV-1. ps20$^{+/+}$ and ps20$^{-/-}$ mice were infected intranasally with 5×10^3 PFU of

MHV-1, a sub-lethal dose in C57Bl/6 mice, and lung viral titers were measured in time course studies. Consistent with what we observed *in vitro*, ps20$^{-/-}$ mice are more susceptible to MHV-1 infection than ps20$^{+/+}$ mice (Fig. 4A). Differences in viral burden in the lungs are evident on days 1 and 2 post-infection (Day 1: ps20$^{+/+}$ ~ 131.5 PFU/g; ps20$^{-/-}$ ~ 2.14×10^4 PFU/g; Day 2: ps20$^{+/+}$ ~ 1.80×10^3 PFU/g; ps20$^{-/-}$ ~ 1.06×10^4 PFU/g.). Notably, we do not observe any weight changes in the mice. By day 4, as mice begin to clear infection, lung viral titers become indistinguishable between the ps20$^{+/+}$ and ps20$^{-/-}$ mice. Additionally, we observe an IFN response to MHV-1 infection in the lungs of infected mice, with no difference in IFN gene expression levels between ps20$^{+/+}$ and ps20$^{-/-}$ mice (Fig. 4B). In the absence of experimental data that show the effects of different lung viral titers on IFN induction, we infer that the viral burden in the lungs of both ps20$^{-/-}$ and ps20$^{+/+}$ mice is such that IFN induction is comparable. Notably ps20$^{-/-}$ mice express significantly higher levels of CXCL1 and CXCL2 mRNA in their lungs in comparison to ps20$^{+/+}$ mice on day 1 post-infection.

MHV-1 virulence is characterized by the immune response to the infection (Albuquerque et al., 2006; Khanolkar et al., 2009a,b). Accordingly, in the next series of experiments we examined the influence of ps20 expression on the immune cell response in the lung draining (d) LNs of ps20$^{+/+}$ and ps20$^{-/-}$ mice at various times post-intranasal infection with MHV-1. On days 2, 4, 6 and 8 post-infection we observed no significant differences in the F4/80$^+$, CD3$^+$-CD4$^+$, CD3$^+$CD8$^+$ or B220$^+$ cell populations between ps20$^{+/+}$ and ps20$^{-/-}$ mice (Supplementary Fig. 2). On day 2 post-infection, we identified an increase in the percentage of GR1$^+$ cells (neutrophils) in the dLNs of ps20$^{-/-}$ mice compared with ps20$^{+/+}$ mice (ps20$^{+/+}$ ~ 27.1%; ps20$^{-/-}$ ~ 47.9) (Fig. 5A). Specifically, the mean absolute GR1$^+$ cell number in the dLN of ps20$^{-/-}$ mice on day 2 was two times greater than in ps20$^{+/+}$ mice (ps20$^{+/+}$ ~ 4.06×10^5 GR1$^+$ cells; ps20$^{-/-}$ ~ 1.07×10^6 GR1$^+$ cells). By day 4 the GR1$^+$ cell numbers were indistinguishable between the ps20$^{+/+}$ and ps20$^{-/-}$ mice (ps20$^{+/+}$ ~ 2.37×10^6 GR1$^+$ cells; ps20$^{-/-}$ ~ 2.59×10^6 GR1$^+$ cells).

To determine whether this increase in GR1$^+$ neutrophils in the lung dLNs of ps20$^{-/-}$ mice was reflective of enhanced neutrophil infiltration into the bronchial alveoli, the BAL was examined for immune cell infiltrates. An increase in the percentage of GR1$^+$ cells infiltrating into the lung of ps20$^{-/-}$ mice was observed on day 2 post-infection (ps20$^{+/+}$ ~ 27.3%; ps20$^{-/-}$ ~ 49.7%) (Fig. 5B). Similar to the dLNs, the mean absolute GR1$^+$ cell number present in the BAL of ps20$^{-/-}$ mice was likewise two times greater than in ps20$^{+/+}$ mice on day 2 (ps20$^{+/+}$ ~ 9.70×10^4 GR1$^+$ cells; ps20$^{-/-}$ ~ 1.78×10^5 GR1$^+$ cells). We observed no differences in other immune cell populations infiltrating into the lung on either day 1 or day 2 post-infection (Supplementary Fig. 2).

A/J mice are more susceptible to MHV-1 infection compared to C57Bl/6 mice (Albuquerque et al., 2006; Khanolkar et al., 2009a). To assess the role of ps20 in MHV-1 infection of A/J mice, mice were pre-treated with the anti-ps20 FAb fragmented antibody IG7 at either 2 or 6 h prior to MHV-1 infection. Treatment with anti-ps20 IG7 FAb resulted in increased viral titers in the lung tissue (2 h: PBS ~ 1.38×10^5 PFU/g; IgG ~ 8.88×10^4 PFU/g; IG7 ~ 9.03×10^5 PFU/g. 6 h: PBS ~ 1.45×10^5 PFU/g; IgG ~ 1.02×10^5 PFU/g; IG7 ~ 6.22×10^5 PFU/g) (Fig. 6).

3.4. ps20 does not affect neutrophil elastase activity

Elafin and SLPI inhibit neutrophil elastase activity, mediated by their WAP domain. (Bouchard et al., 2006; Doumas et al., 2005; Sallenave et al., 1997). Neutrophil elastase activity enables neutrophils to permeate the vascular basement membrane and migrate into sites of inflammation (Wang et al., 2005; Young et al., 2007). Given that ps20 contains the conserved WAP domain, we under-
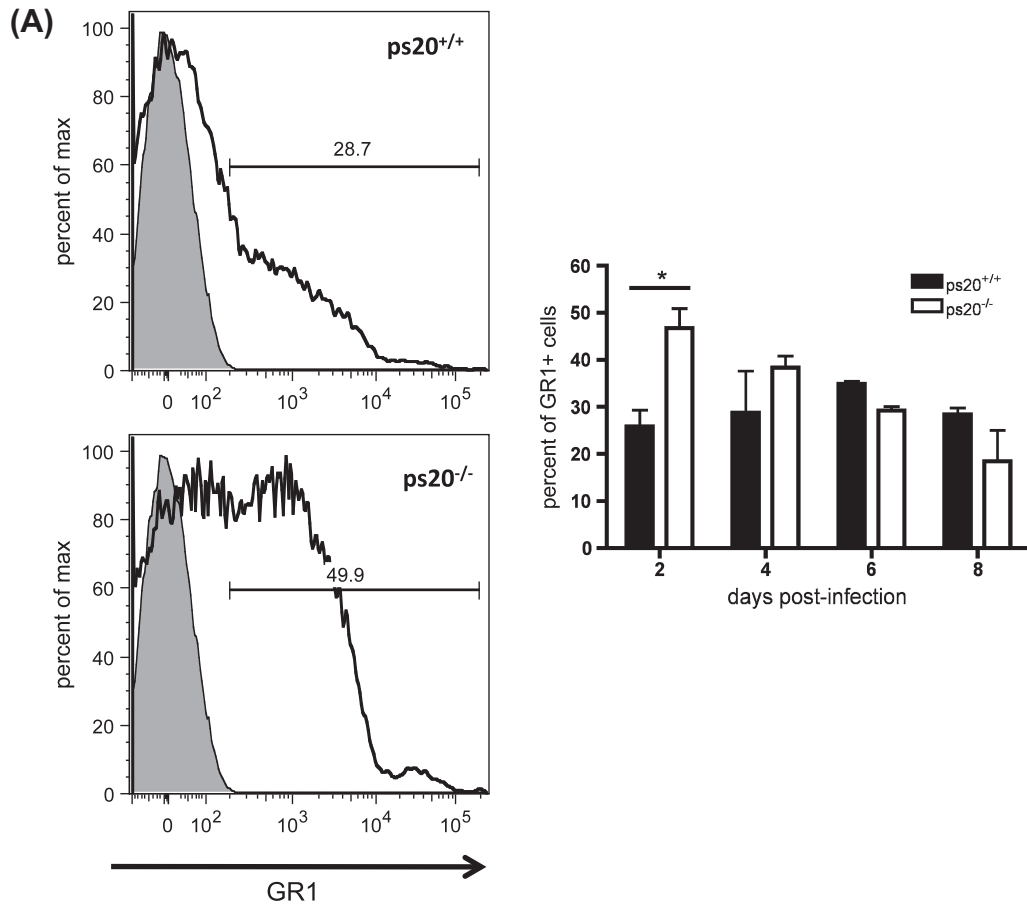
Fig. 5. ps20 affects neutrophil lymph node accumulation accompanying MHV-1 infection. Female ps20$^{+/+}$ and ps20$^{-/-}$ mice aged 6–8 weeks were infected by intranasal instillation with 5×10^3 PFU of MHV-1. Mice were sacrificed at the indicated time points and their lungs, dLNs and BAL harvested as described in Section 2.3. Cells were isolated and stained for lineage specific cell markers. (A) Representative plots of the mean fluorescent intensity of GR1$^+$ (APC-Cy7) cells isolated from the dLN of both ps20$^{+/+}$ (top left) and ps20$^{-/-}$ (lower left) mice on day 2 post-infection. The histograms represent the mean of the GR1$^+$ population in the dLN at the indicated time points ± standard error ($n = 3$ for each group). (B) Representative plots of the mean fluorescent intensity of GR1$^+$ (APC-Cy7) cells isolated from the BAL of a ps20$^{+/+}$ (top left) or ps20$^{-/-}$ (lower left) mice on day 2 post-infection. The histogram represents the mean of the GR1$^+$ population in the BAL at the indicated time points ($n = 3$ for each group). Gates were set based on isotype-matched antibodies. The data are representative of one (1, and 4–8 days post-infection) or two (2 days post-infection) independent experiments and were analyzed using a Student's t test. $^*P < 0.05$.

took a series of experiments to determine whether ps20 inhibits neutrophil elastase activity, thereby limiting neutrophil entry into sites of MHV-1 infection. In dose–response experiments we examined the ability of recombinant ps20 protein, when incubated with human neutrophil elastase, to affect the elastase cleavage of the substrate N-methoxysuccinyl-Ala-Ala-Pro-Val p-nitroanilide. Neutrophil elastase cleaves the substrate on the carboxyl side of valine and this cleavage results in the liberation of p-nitroanilide (Hagio et al., 2001; Simpson et al., 2001). Whereas 10 µg/mL of elafin effectively inhibited neutrophil elastase activity by greater than 98%, up to 100 µg/mL of ps20 had no effect (Fig. 7A).

3.5. ps20$^{-/-}$ neutrophils are more susceptible to MHV-1 infection

Given the increase in neutrophil infiltrates in the lungs of MHV-1 infected ps20$^{-/-}$ mice we undertook a series of experiments to further address their contribution to enhanced infectivity. Neutrophils were isolated from the BM of ps20$^{+/+}$ and ps20$^{-/-}$ mice and cell surface expression of CEACAM-1, the receptor for MHV-1, was determined by FACS. The data in Fig. 8A identify cell surface expression of CEACAM-1 in both ps20$^{+/+}$ and ps20$^{-/-}$ neutrophils, at comparable levels. The implications are that MHV-1 will infect neutrophils. Accordingly, we examined the infectivity of BM derived neutrophils from ps20$^{+/+}$ and ps20$^{-/-}$ mice and provide evi-

dence that both are susceptible to MHV-1 infection, yet the absence of ps20 is associated with greater infectivity (Fig. 8B). Neutrophils are generally associated with clearance of infectious pathogens, mediated by their TLR activation and generation of reactive oxygen species (ROS) and neutrophil extracellular traps (NETs) (Clark et al., 2007; Gonzalez-Dosal et al., 2011). Notably, exposure of both ps20$^{+/+}$ and ps20$^{-/-}$ BM derived neutrophils to MHV-1 did not result in intracellular ROS generation and neutrophils from ps20$^{-/-}$ mice have lower levels of intracellular ROS even in the absence of infection (Fig. 8C). Immunohistology of lungs from ps20$^{+/+}$ and ps20$^{-/-}$ mice infected with MHV-1 did not reveal NET formation at 48 h post-infection, despite evidence of extensive neutrophil lung infiltration (Fig. 9).

4. Discussion

At the outset of these studies we established a colony of ps20$^{+/+}$ and ps20$^{-/-}$ mice, backcrossed to > 98% homogeneity onto a C57Bl/6 background. Our initial experiments focused on characterizing the immune compartments of the ps20$^{-/-}$ mice, in the context of profiling different immune cell populations. We examined the PB, spleen, LNs, and BM. The neutrophil population circulating in the PB is increased in the ps20$^{-/-}$ mice compared with ps20$^{+/+}$ mice. Examination of other immune cell compartments identified no dif-
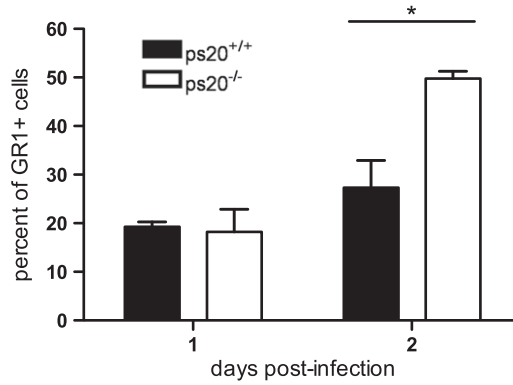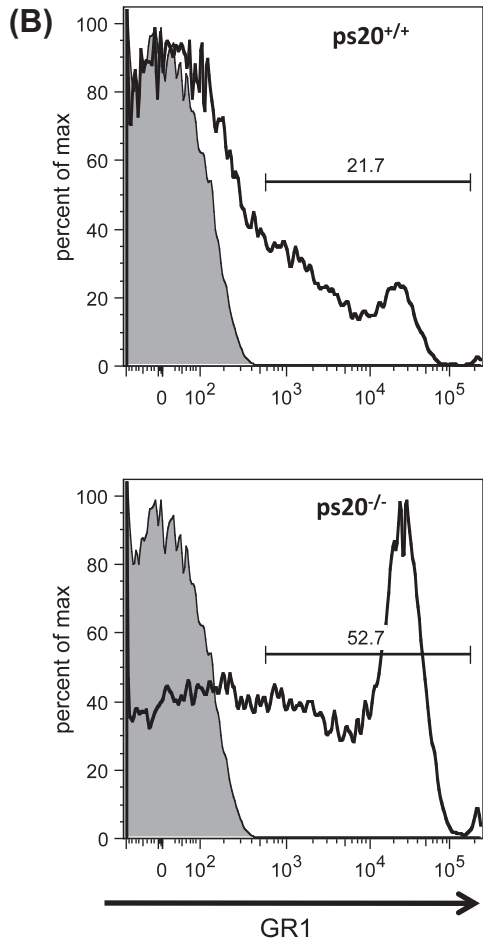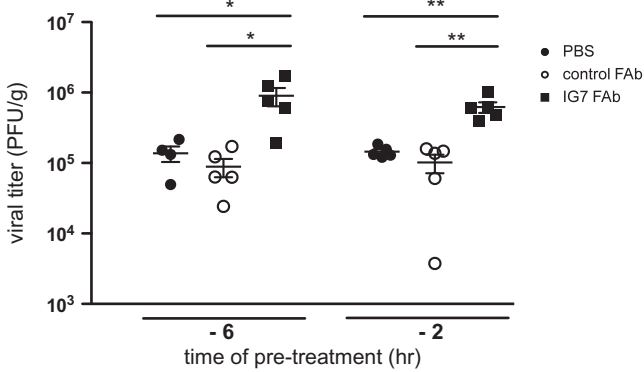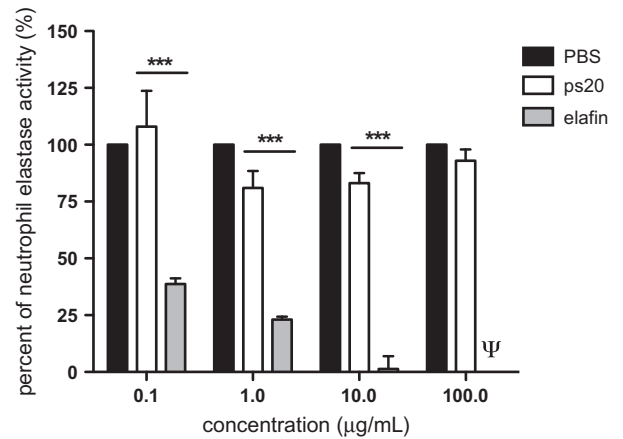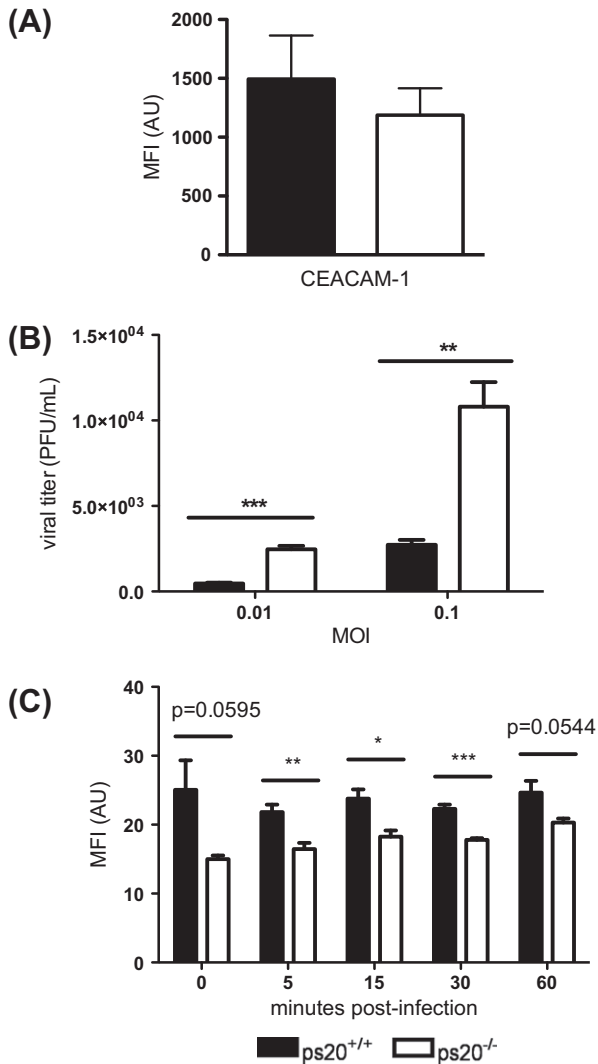
(B)

Fig. 5. (*continued*)

Fig. 6. Antibody targeting of ps20 affects susceptibility to MHV-1 infection. Female A/J mice aged 6–8 weeks were treated by intranasal instillation with 100 µg of either a control IgG FAb or the ps20-specific IG7 FAb, at 2 or 6 h before intranasal infection with MHV-1 (5×10^3 PFU). 24 h post-infection, mice were sacrificed and their lungs harvested for viral titration as described in Section 2.5. The data are presented as PFU/g of lung tissue for each mouse, with the mean of each group ($n = 5$) indicated by the solid black line and are representative of two independent experiments. Data were analyzed using a Student's t test. $^*P < 0.05$; $^{**}P < 0.01$.

Fig. 7. ps20 does not inhibit neutrophil elastase activity. Human neutrophil elastase was incubated with log-fold dilutions of human elafin, or recombinant human ps20 in individual wells of a 96 well plate, for 30 min. *N*-methoxysuccinyl-Ala-Ala-Pro-Val p-nitroanilide was then added for a further 15 min, then absorbance measurements recorded at 405 nm. Data are plotted such that the background absorbance of the negative control (no neutrophil elastase) was subtracted from the mean absorbance value for each group ($n = 4$). PBS (no inhibitor) is considered as the 100% activity level for elastase activity. Ψ indicates not done. The data are representative of two independent experiments analyzed by a Student's t test. $^{***}P < 0.001$.

ferences in the abundance of neutrophils. Indeed, the numbers and proportions of other leukocyte populations, including F4/80^{+} macrophages, CD3^{+}CD4^{+} and CD3^{+}CD8^{+} T cells, B220^{+} B cells or NK1.1^{+} NK cells, are indistinguishable between ps20^{+/+} and ps20^{−/−} mice for all compartments examined.
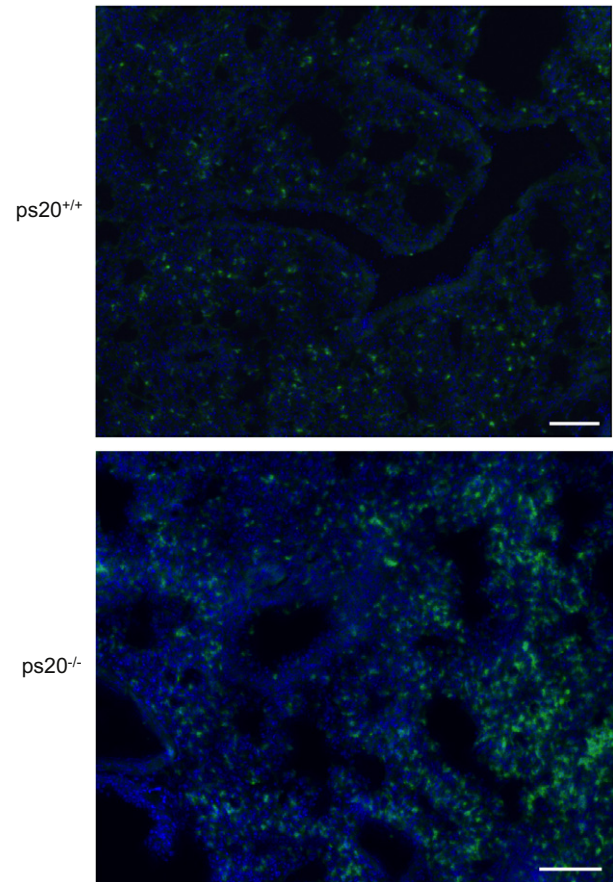
Previously published studies describing the role of ps20 in viral infections have focused on HIV infection, where ps20 has been

(A)

(B)

(C)

Fig. 9. Evidence of neutrophil infiltrates in MHV-1 infected lungs. Female ps20^{+/+} (n = 3) and ps20^{−/−} (n = 3) mice aged 6–8 weeks were infected by intranasal instillation with 5×10^3 PFU of MHV-1. Mice were sacrificed 48 h post-infection and lungs were harvested for immunohistology: stained with DAPI (blue) and anti-Ly6G (green) as described in Section 2.10. Images are representative of multiple lung sections at each time point.

Fig. 8. Neutrophils are susceptible to MHV-1 infection. Neutrophils were harvested from the BM of ps20^{+/+} and ps20^{−/−} mice and infected with MHV-1 at MOIs of 0.01 and 0.1 for 24 h, then viral titers determined as described in Section 2.5. (A) CEACAM-1 expression on ps20^{+/+} and ps20^{−/−} neutrophils prior to MHV-1 infection. Data are presented as mean fluorescence intensity (MFI) and are representative of three independent experiments. (B) Viral titer. Data are presented as PFU/mL for each group (n = 3) ± standard error and are representative of three independent experiments. Data were analyzed by using a Student's t test. **$P < 0.01$; ***$P < 0.001$. (C) Neutrophils harvested from the BM of ps20^{+/+} and ps20^{−/−} mice were incubated with H$_2$DCFDA for 30 min. prior to infection with MHV-1 at an MOI of 0.01 for the indicated times. Intracellular ROS was quantitated by FACS analysis. Data are presented as the MFI ± standard error and are representative of two independent experiments. Data were analyzed by using a Student's t test. *$P < 0.05$; **$P < 0.01$; ***$P < 0.001$.

identified as a HIV dependency factor in *in vitro* assay systems (Alvarez et al., 2007; Bingle and Vyakarnam, 2008). An objective of our studies was to interrogate the effects of ps20 in another virus infection, namely respiratory MHV-1. *In vitro*, we provide evidence that ps20^{−/−} fibroblasts are infected to a greater extent than ps20^{+/+} fibroblasts and anti-ps20 FAb treatment renders cells more susceptible to infection. MHV-1 infection of ps20^{+/+} and ps20^{−/−} mice confirmed our *in vitro* findings, providing evidence that the absence of ps20 expression results in enhanced lung infection. Moreover, when A/J mice were pre-treated with an anti-ps20 FAb fragment, IG7, prior to infection with MHV-1, where the IG7 antibody targets the C-terminal portion of ps20, we observed enhanced lung viral infectivity.

A role for ps20 as an antiviral agent against MHV-1 infection is in agreement with the antiviral properties of elafin and SLPI. SLPI mediates its antiviral activity against HIV by binding annexin II and blocking phosphatidylserine binding and entry in macrophages (Ma et al., 2004). The antiviral activity of SLPI appears to be independent of its serine protease activity (McNeely et al., 1995). Although not shown to be the case in the context of HIV and elafin, the anti-bacterial and anti-fungal effects of elafin are also independent of serine protease activity (Baranger et al., 2008; Ghosh et al., 2009).

In vitro, we provide evidence that MHV-1 infection induces an IFN response in both ps20^{+/+} and ps20^{−/−} fibroblasts, albeit to a lesser extent in ps20^{−/−} fibroblasts, and that IFN-α4 treatment protects ps20^{−/−} fibroblasts from MHV-1 infection, suggesting that IFN-inducible signaling events are unaffected in the absence of ps20 expression. *In vivo*, we show that MHV-1 infection likewise induces an IFN response in lung tissues in both ps20^{+/+} and ps20^{−/−} mice. Our data suggest that viral induction of IFN gene expression is unaffected by ps20, since the direct association of viral load with inducible IFN gene expression is intact.

In vivo, we observe that on day 2 post-infection there is a greater influx of neutrophils in the BAL and lung dLNs of ps20^{−/−} compared with ps20^{+/+} mice. No other differences were observed for other leukocyte populations, in either the BAL or dLNs. Since neutrophils express CEACAM-1 and therefore are potentially susceptible to infection by MHV-1 (Godfraind et al., 1995), an intriguing

possibility was that enhanced neutrophil infiltration into the lungs of the $ps20^{-/-}$ mice results in greater infectivity with MHV-1 associated with neutrophil infection. We show that BM derived neutrophils from $ps20^{+/+}$ and $ps20^{-/-}$ mice express cell surface CEACAM-1 to similar levels and are indeed readily infected by MHV-1. We provide evidence that the $ps20^{-/-}$ neutrophils are more susceptible to MHV-1 infection than the $ps20^{+/+}$ neutrophils. In addition, we observe that exposure of neutrophils to MHV-1 did not result in the generation of ROS that are associated with the anti-microbial activity of neutrophils. Moreover, in contrast to published data that describe a role for neutrophil extracellular traps (NET) contributing to acute lung injury in influenza pneumotitis (Narasaraju et al., 2011), extensive examination of infected lung tissue did not show NETs (Fig. 9).

The increased number of neutrophils in the circulation of $ps20^{-/-}$ mice could be the result of a number of factors. Since neutrophil elastase activity facilitates the migration of neutrophils into inflamed tissue (Wang et al., 2005; Young et al., 2007), we speculated that ps20 may inhibit elastase activity, resembling elafin and SLPI, and that this inhibitory activity might decreased neutrophil migration into the lungs of $ps20^{+/+}$ mice compared with $ps20^{-/-}$ mice. However, in vitro examination of ps20 effects on neutrophil elastase activity revealed no inhibition. Close examination of the signature amino acid sequence conserved in SLPI and elafin that is thought to be associated with neutrophil elastase activity, reveals that it is not conserved in ps20 (Bingle and Vyakarnam, 2008). Accordingly, the difference observed in neutrophil migration between $ps20^{+/+}$ and $ps20^{-/-}$ mice during MHV-1 infection likely is not a consequence of ps20 effects on neutrophil elastase activity.

Neutrophil migration is effected by the chemokines CXCL1 and CXCL2, chemoattractants for neutrophils that express the cognate receptor, CXCR2 (Bozic et al., 1994). CXCL1 and CXCL2 promote neutrophil migration and cell adhesion, by invoking the modification of several integrins (Seo et al., 2001). Examination of gene expression levels for these chemokines in the $ps20^{+/+}$ and $ps20^{-/-}$ fibroblasts following MHV-1 infection revealed greater CXCL1 and CXCL2 expression in the $ps20^{-/-}$ fibroblasts. Furthermore, in vivo, we observe elevated gene expression levels of both CXCL1 and CXCL2 in the lungs of $ps20^{-/-}$ mice in comparison to $ps20^{+/+}$ mice on day 1 post-infection with MHV-1. These findings implicate ps20 as a potential regulatory factor that limits the expression of neutrophil specific chemotactic factors, CXCL1 and CXCL2.

Viewed altogether, the data support a role for ps20 as a host factor that regulates the innate immune response to virus infections. For HIV, accumulating data suggest that ps20 influences T cell responses to infection, promoting infection. For MHV-1, our data describe a role for ps20 in limiting neutrophil accumulation in affected lungs, thereby providing protection from infection. Given the profoundly different consequences associated with ps20 expression in HIV and MHV-1 infections, our ongoing studies are directed towards elaborating the spectrum of activity of ps20 in the regulation of immune cell activation and trafficking. The intent is to consider this regulation in the context of specific virus infections that are regarded as a global health threat, and to develop strategies that invoke targeting ps20 for therapeutic intervention where relevant.

Funding

Appendix A. Supplementary data

Supplementary data associated with this article can be found, in the online version, at http://dx.doi.org/10.1016/j.antiviral.2012.08.012.

References

Albuquerque, N.D., Baig, E., Ma, X., Zhang, J., He, W., Rowe, A., Habal, M., Liu, M., Shalev, I., Downey, G.P., Gorczynski, R., Butany, J., Leiboqitz, J., Weiss, S., McGilvray, I.D., Phillips, M.J., Fish, E.N., Levy, G.A., 2006. Murine hepatitis virus strain 1 produces a clinically relevant model of Severe acute respiratory syndrome in A/J mice. J. Virol. 80, 10382–10384.

Alvarez, R., Reading, J., King, D.F.L., Hayes, M., Easterbrook, P., Farzaneh, F., Ressler, S., Yang, F., Rowley, D., Vyakarnam, A., 2007. WFDC1/ps20 is a novel innate immunomodulatory signature protein of human immunodeficiency virus (HIV)-permissive CD4+CD45RO+ memory T cells that promotes infection by upregulating CD54 integrin expression and is elevated in HIV type 1 infection. J. Virol. 82, 471–486.

Baig, E., Fish, E.N., 2008. Distinct signature type I interferon responses are determined by the infecting virus and the target cell. Antivir. Ther. 13, 409–422.

Baranger, K., Zani, M.L., Chandenier, J., Dallet-Choisy, S., Moreau, T., 2008. The antiacterial and antifungal properties of trappin-2 (pre-elafin) do not depend on its protease inhibitory function. FEBS J. 275, 2008–2020.

Bingle, C.D., Vyakarnam, A., 2008. Novel innate immune functions of the whey acidic protein family. Trends Immunol. 29, 444–453.

Bingle, L., Tetley, T., Bingle, C.D., 2001. Cytokine-mediated induction of the human elafin gene in ulmonary epithelial cells is regulated by nuclear-factor-kB. Am. J. Respir. Cell Mol. Biol. 25.

Bouchard, D., Morisset, D., Bourbonnais, Y., Tremblay, G.M., 2006. Proteins with whey-acidic-protein motifs and cancer. Lancet Oncol. 7, 167–174.

Bozic, C.R., Gerard, N.P., von Uexkull-Guldenband, C., Kolakowski, L.F., Conklin, M.J., Breslow, R., Showell, H.J., Gerard, C., 1994. The murine interleukin 8 type B receptor homologue and its ligands. J. Biol. Chem. 269, 29355–29358.

Clark, S.R., Ma, A.C., Tavener, S.A., McDonald, B., Goodarzi, Z., Kelly, M.M., Patel, K.D., Chakrabarti, S., McAvoy, E., Sinclair, G.D., Keys, E.M., Allen-Vercoe, E., Devinney, R., Doig, C.J., Green, F.H., Kubes, P., 2007. Platelet TLR4 activates neutrophil extracellular traps to ensnare bacteria in septic blood. Nat. Med. 13, 463–469.

Compton, S.R., Stephensen, C.B., Snyder, S.W., Wismiller, D.G., Holmes, K.V., 1992. Coronavirus species specificity: murine coronavius binds to a mouse-specific epitope on its carcinoembryonic antigen-related receptor glycoprotein. J. Virol. 66.

Doumas, S., Kolokotronis, A., Stefanopoulos, P., 2005. Anti-inflammatory and antimicrobial roles of secretory leukocyte protease inhibitor. Infect. Immun. 73, 1271–1274.

Fish, E.N., Hannigan, G.E., Banerjee, K., Williams, B.R., 1988. The interaction of interferon-alpha and -gamma: regulation of (2–5)A synthetase activity. Virology 165, 87–94.

Ghosh, M., Shen, Z., Fahey, J.V., Cu-Uvin, S., Mayer, K., Wira, C.R., 2009. Trappin-2/Elafin: a novel innate anti-human immunodeficiency virus-1 molecule of the human female reproductive tract. Immunology 129, 207–219.

Godfraind, C., Langreth, S.G., Cardellichio, C.B., Knobler, R., Coutelier, J.P., Dubois-Dalcq, M., Holmes, K.V., 1995. Tissue and cellular distribution of an adhesion molecule in the carcinoembryonic antigen family that serves as a receptor for mouse hepatitis virus. Lab. Invest. 73, 615–627.

Gonzalez-Dosal, R., Horan, K.A., Rahbek, S.H., Ichijo, H., Chen, Z.J., Mieyal, J.J., Hartmann, R., Paludan, S.R., 2011. HSV infection induces production of ROS, which potentiate signaling from pattern recognition receptors: role for S-glutathionylation of TRAF3 and 6. PLoS Pathog. 7, e1002250.

Gu, J., Korteweg, C., 2007. Pathology and pathogenesis of severe acute respiratory syndrome. Am. J. Pathol. 170, 1136–1147.

Hagio, T., Nakao, S., Matsuka, H., Matsumoto, S., Kawabata, K., Ohno, H., 2001. Inhibition of neutrophil elastase activity attenuates complement-mediated lung injury in the hamster. Eur. J. Pharmacol. 426, 131–138.

Hennighausen, L.G., Sippel, A.E., 1982a. Comparative sequence analysis of the mRNAs coding for mouse and rat whey protein. Nucleic Acids Res. 10, 3733–3744.

Hennighausen, L.G., Sippel, A.E., 1982b. Mouse whey acidic protein is a novel member of the family of 'four-disulfide core' proteins. Nucleic Acids Res. 10, 2677–2684.

Khanolkar, A., Hartwig, S.M., Haag, B.A., Meyerholz, D.K., Epping, L.L., Haring, J.S., Varga, S.M., Harty, J.T., 2009a. Protective and pathologic roles of the immune response to mouse hepatitis virus type 1: implications for severe acute respiratory syndrome. J. Virol. 83, 9258–9272.

Khanolkar, A., Hartwig, S.M., Haag, B.A., Meyerholz, D.K., Harty, J.T., Varga, S.M., 2009b. Toll-like receptor 4 deficiency increases disease and mortality after mouse hepatitis virus type I infection of suscptible C3H mice. J. Virol. 83, 8946–8956.

Larsen, M., Ressler, S.J., Gerdes, M.J., Lu, B., Byron, M., Lawrence, J.B., Rowley, D.R., 2000. The WFDC1 gene encoding ps20 localizes to 16q24, a region of LOH in multiple cancers. Mamm. Genome 11, 767–773.

Ma, G., Greenwell-Wild, T., Lei, K., Jin, W., Swisher, J., Hardegen, N., Wild, C.T., Wahl, S.M., 2004. Secretory leukocyte protease inhibitor binds to annexin II, a cofactor for macrophage HIV-1 infection. J. Exp. Med. 200, 1337–1346.

McNeely, T.B., Ddealy, M., Dripps, D.J., Orenstein, J.M., Eisenbery, S.O., Wahl, S.M., 1995. Secretory leukocyte protease inhibitor: a human saliva protein exhibiting anti-human immunodeficiency virus 1 activity in vitro. J. Clin. Invest. 96, 456–464.

Narasaraju, T., Yang, E., Samy, R.P., Ng, H.H., Poh, W.P., Liew, A.A., Phoon, M.C., van Rooijen, N., Chow, V.T., 2011. Excessive neutrophils and neutrophil extracellular traps contribute to acute lung injury of influenza pneumonitis. Am. J. Pathol. 179, 199–210.

Perlman, S., Netland, J., 2009. Coronaviruses post-SARS: update on replication and pathogenesis. Nat. Rev. Microbiol. 7, 439–450.

Piletz, J.E., Heinlen, M., Ganschow, R.E., 1981. Biochemical characterization of a novel whey proteins from murine milk. J. Biol. Chem. 256, 11509–11516.

Sallenave, J., Si-Tahar, M., Cox, G., Chignard, M., Gauldie, J., 1997. Secretory leukocyte elastase inhibitor in human neutrophils. J. Leukoc. Biol. 61, 695–702.

Seo, S.M., McIntire, L.V., Smith, W., 2001. Effects of IL-8, gro-alpha, and LTB4 on the adhesive kinetics of LFA-1 and mac-1 on human neutrophils. Am. J. Physiol. 281, 1568–1578.

Simpson, K.J., Nicholas, K.R., 2002. The comparative biology of whey proteins. J. Mammary Gland Biol. Neoplasia 7, 313–326.

Simpson, A.J., Wallace, W.A., Marsden, M.E., Govan, J.R., Porteous, D.J., Haslett, C., Sallenave, J.M., 2001. Adenoviral augmentation of elafin protects the lung against acute injury mediated by activated neutrophils and bacterial infection. J. Immunol. 167, 1778–1786.

Simpson, K.J., Ranganathan, S., Fisher, J.A., Janssens, P.A., Shaw, D.C., Nicholas, K.R., 2000. The gene for a novel member of the whey acidic protein family encodes three four-disulfide core domains and is asynchronously expressed during lactation. J. Biol. Chem. 275, 23074–23081.

Spaan, W., Cavanagh, D., Horzinek, M.C., 1988. Coronaviruses: Structure and Genome Expression. J. Gen. Virol. 69, 2939–2952.

Wang, S., Dangerfield, J.P., Young, R.E., Nourshargh, S., 2005. PECAM-1, alpha6, integrins and neutrophil elastase cooperate in mediating neutrophil transmigration. J. Cell Sci. 118, 2067–2076.

Young, R.E., Voisin, M.B., Wang, S., Dangerfield, J.P., Nourshargh, S., 2007. Role of neutrophil elastase in LTB4-induced neutrophil transmigration in vivo assessed with a specific inhibitor and neutrophil elastase deficient mice. Br. J. Pharmacol. 151, 628–637.

Zhou, H., Perlman, S., 2007. Mouse hepatitis virus does not induce beta interferon synthesis and does not inhibit its induction by double-stranded RNA. J. Virol. 81, 568–574.

Zorzitto, J., Galligan, C.L., Ueng, J.J., Fish, E.N., 2006. Characterization of the antiviral effects of interferon-alpha against a SARS-like coronavirus infection in vitro. Cell Res. 16, 220–229.

Glossary

BAL: bronchial alveolar lavage
BM: bone marrow
BSA: bovine serum albumin
CEACAM-1: carcinoembryonic antigen-related cell adhesion molecule 1
CPE: cytopathic effect
CXCL1: chemokine (C–X–C motif) ligand 1
CXCL2: chemokine (C–X–C motif) ligand 2
CXCR2: chemokine (C–X–C motif) receptor 2
DAPI: 4′-6-Diamidino-2-phenylindole
dLN: draining lymph node
DMEM: Dulbecco's modified Eagle's medium
ELISA: enzyme-linked immunosorbent assay
FAb: fragmented antibody
FACS: fluorescence activated cell sorting
FCS: fetal calf serum
FDC: four disulfide core
FSC: forward scatter
HIV: human immunodeficiency virus
HPRT: hypoxanthine phosphoribosyltransferase
IFN: interferon
IFN-a4: interferon alpha-4
IFN-β: interferon beta
ip: intraperitoneal
ISG15: interferon-stimulated gene 15 kDa
LN: lymph node
mAb: monoclonal antibody
MFI: mean fluorescence intensity
MHV-1: mouse hepatitis virus type 1
MOI: multiplicity of infection
NET: neutrophil extracellular trap
PB: peripheral blood
PBMC: peripheral blood mononuclear cell
PFU: plaque forming unit
ROS: reactive oxygen species
SSC: side scatter
SLPI: secretory leukocyte protease inhibitor
WAP: whey acidic protein